BIOCHE 1825

Renormalization of hydration forces by collective protrusion modes

Reinhard Lipowsky and Stefan Grotehans

Institut für Festkörperforschung Forschungszentrum Jülich, Postfach 1913, W-5170 Jülich (Germany)

Abstract

Lipid membranes which interact via direct hydration forces and which exhibit thermally excited protrusions are studied in the framework of interface models. These models are studied by functional renormalization group methods which predict two different interaction regimes: (i) a protrusion-dominated regime for sufficiently high temperature, and (ii) a hydration-dominated regime for sufficiently low temperature. These predictions are fully confirmed by Monte Carlo simulations. It is also shown that the protrusion-induced roughness of the lipid water interfaces acts to reduce the bending rigidity.

Keywords: Lipid membranes; Hydration forces; Protrusion; Monte Carlo simulation

1. Introduction

The interaction between lipid bilayers and other flexible membranes is governed by the interplay between direct molecular forces and entropic forces arising from thermally excited fluctuations (for recent reviews, see ref. [1]). On length scales which are large compared to the membrane thickness, the typical fluctuations are expected to be bending modes for which the surface area of the membrane remains unchanged. On length scales which are comparable to or smaller than the membrane thickness, on the other hand, the membrane will be roughened by protrusion modes, i.e. by the relative displacements of the lipid molecules [2–6]. These latter fluctuations change the surface area of the membrane.

From the theoretical point of view, bending modes act to renormalize the long-ranged van der Waals or other long-ranged forces [1]. Protrusion modes, on the other hand, renormalize the short-ranged forces as will be explained in this paper (a short report of some of our results will be given elsewhere [7]).

The interaction of lipid bilayers can be experimentally studied by a variety of techniques (for a review, see ref. [8]): (i) using crossed mica cylinders, the separation of two bilayers immobilized on these cylinders can be measured as a function of the applied force between their surfaces [9]; (ii) the cohesion of two large vesicles can be controlled by micropipettes and observed by phase contrast microscopy (for a review, see ref. [10]); (iii) accidental cohesive contacts within membrane bundles can also be studied by optical

microscopy [11], and (iv) the separation of bilayers within multilayer systems can be measured by X-ray or neutron scattering as a function of the applied osmotic pressure [8].

It has been found from the multilayer measurements that lipid bilayers exhibit a strong repulsive force at separations of the order of 1 nm. The force per unit area or disjoining pressure, P, has been observed to decay exponentially as $P \approx P_t \exp[-\ell/l_t]$ with the mean separation ℓ of the two membranes (here and below, the subscript t stands for "total"). The experimentally determined decay length l_t varies from 0.1 to 0.3 nm; the measured amplitude P_t of this pressure is rather large and is estimated to be in the range $4 \times 10^7 \leqslant P_t \leqslant 4 \times 10^9$ J/m^3.

A similar short-ranged and repulsive force was found for bilayers immobilized on mica surfaces. However, the functional dependence of the bilayer separation on the force as obtained for the immobilized membranes is somewhat different from the one obtained for the multilayer systems [12].

If the immobilized bilayers are firmly attached to the mica surfaces, they should not undergo any shape fluctuations and their interactions should be determined only by the direct molecular forces. Here, we will consider lipid bilayers which are not charged and which do not interact via macromolecules or colloids. The direct interaction of these membranes is then given by repulsive hydration forces and attractive van der Waals forces. We will focus on short separations of the order of 1 nm for which the repulsive hydration interaction dominates.

1.1. Hydration length

The hydration interaction is believed to arise from the intrinsic structure of the two lipid water interfaces bounding the intermediate water layer. The density used to describe these interfaces could be the local polarization of the water molecules [13] or an order parameter which describes the hydrogen bonds [14].

In order to give a precise definition of the hydration length, consider a membrane which has been immobilized on a planar surface. The lipid water interface of such a bilayer is characterized by a density profile which represents the lateral average of the local density and thus depends only on the coordinate, say y, perpendicular to this interface.

If the lipid water interface were smooth and planar on the scale of the water molecules, the density profile would exhibit oscillations which represent the successive packing of planar water layers on top of the lipid bilayer. However, the surface of the immobilized bilayer is rough on the scale of the water molecules since it exhibits 'hills' and 'valleys', the size of which is set by the lipid head groups. Therefore, the water layers are corrugated and the lateral average leads to a density profile for which the oscillatory part is strongly suppressed. The decay of this profile should then be characterized by an exponential tail $\sim \exp(-y/l_{hy})$ which defines the hydration length l_{hy}.

If two such immobilized bilayers are pushed against each other by the external pressure P, the density profiles of their surfaces overlap. This leads to a repulsive interaction of the form $\sim \exp(-l/l_{hy})$ between these two lipid water interfaces, where l denotes their separation. This interaction is consistent with surface force measurements for bilayers immobilized on mica surfaces (for which an oscillatory behavior has not been observed) [6,12]. Thus, the interaction potential $V(l)$ has the generic form

$$V(l) = V_{hw}(l) + V_{hy} \exp[-l/l_{hy}] + Pl, \qquad (1.1)$$

where the hard wall potential V_{hw} is given by

$$V_{hw}(l) = \infty \quad \text{for} \quad l < 0,$$

$$V_{hw}(l) = 0 \quad \text{for} \quad l > 0. \qquad (1.2)$$

The latter potential ensures that the membranes cannot penetrate each other. In addition, it is useful to include this potential term explicitly since it generates another length scale, namely the protrusion length, via thermally excited protrusions.

1.2. Protrusion length

First, consider a single protrusion mode in which a single lipid molecule pulls out from one of the planar membranes and bridges the intermediate water gap of size l [2]. The lipid molecule is taken to have the shape of a small column with constant crosssection; the area of this crosssection is denoted by A_0 and its circumference by a_0. Such a protrusion has energy $\Delta E = \sigma a_0 l$, where σ represents the free energy of the interface between the nonpolar part of the molecule and the water (or another polar solvent). Now, the probability for such a fluctuation can be estimated by the Boltzmann weight, $\exp(-\Delta E/T) = \exp(-l/l_{sc})$ with the length scale

$$l_{sc} = T/a_0\sigma. \tag{1.3}$$

For a molecule with circumference $a_0 \simeq 3$ nm and interfacial free energy $\sigma \simeq 0.02$ J/m^2, this length scale is $l_{sc} \simeq 0.07$ nm at room temperature with $T = 4.12 \times 10^{-21}$ J.

Thus, the protrusions of the lipid water interface introduce another length scale, the protrusion length l_{pr}. Within the single mode picture, this scale is in fact equal to l_{sc}. In general, one has $l_{pr} = z_{pr} l_{sc}$ with a dimensionless coefficient $z_{pr} > 1$ as will be shown below.

Thus, the interplay between hydration forces and protrusion modes can be understood in terms of two length scales, the hydration length l_{hy} and the protrusion length l_{pr}.

There is, however, one obvious problem with the original picture based on single protrusion modes. Since l_{sc} is of the order of 0.1 nm, a protrusion of a single molecule which bridges a water gap of about 1 nm is very unlikely. In real systems there are, however, two different effects which act to increase the effective range of protrusions: (i) the molecules protrude collectively. If several molecules protrude in a coherent fashion, they can form, e.g., transient ripples which are similar to the frozen ripples of the P_{β}' phase. In this way, collective protrusions can bridge a water layer of 1 nm even though the relative displacements of neighboring molecules are only a few
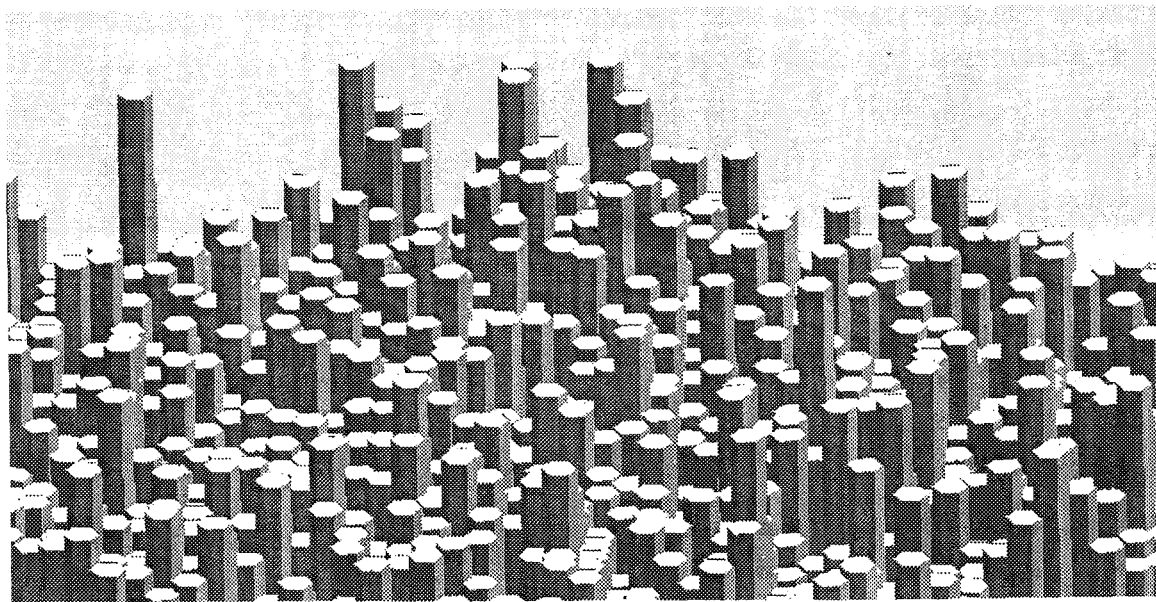

Fig. 1. Snapshot of membrane segment which is roughened by collective protrusion modes. The vertical scale and thus the size of the protrusions have been exaggerated compared to the diameter of the molecules.

angstrom; and (ii) the profile of the water structure in front of the lipid surface is shifted by the protrusions. These two effects will be studied below.

2. Models for collective protrusion modes

We will now go beyond the single mode picture and consider a rough membrane in which all molecules can be displaced with respect to the flat state [7]. A snapshot of such a membrane is shown in fig. 1. In addition, we will include the direct interaction $V(l)$ between the membranes. The separation of the protruding molecule i from the other membrane is now described by the local displacement field l_i which varies along the membrane surface. Each molecule within the membrane is supposed to be in contact with n nearest neighbors. The energy of such a membrane configuration is given by

$$\mathcal{H}\{l\}/T = \sum_{\langle ij \rangle} (a_0\sigma/Tn)\,|l_i - l_j|$$
$$+ \sum_i A_0 V(l_i)/T \qquad (2.1)$$

and its statistical weight is given by the Boltzmann factor $\sim \exp[-\mathcal{H}\{l\}/T]$. Strictly speaking, this model governs the interaction between one bilayer with protrusions and another flat bilayer. However, it can also be used in order to estimate the interaction of two protruding bilayers as discussed at the end [1].

Protrusions change the area of the lipid water interface. Therefore, these fluctuations are governed by an effective interfacial tension. The water layer between two lipid water interfaces then resembles a thin wetting layer. Indeed, an

interface model similar to (2.1) has been previously studied in the context of *wetting* in a lattice gas (or Ising) model. This interface model belongs to the same universality class as the continuum model defined by

$$\mathcal{H}\{l\}/T = \int d^2x \left[\tfrac{1}{2}(\Sigma_{pr}/T)(\nabla l)^2 \right.$$
$$\left. + V(l)/T \right], \qquad (2.2)$$

in which the discrete sites i have been replaced by the continuous coordinate $x = (x_1, x_2)$. The parameter Σ_{pr} represents the effective interfacial tension on large scales; the index pr indicates that this tension arises from protrusions. It will become clear below that

$$\Sigma_{pr} = c_\Sigma(a_0\sigma)^2/T = c_\Sigma T/l_{sc}^2. \qquad (2.3)$$

The Monte Carlo simulations described in section 4 below lead to the estimate $c_\Sigma \simeq 0.067$. Using the above estimate for l_{sc}, one then has $\Sigma_{pr} \simeq 0.056$ J/m².

3. Functional renomalization of continuum interface models

The continuum models as given by (2.2) can be studied by functional renormalization group (RG) methods. It is convenient to start from the nonlinear recursion relation as described in ref. [15] in order to include the hard wall potential $V_{hw}(l)$.

3.1. Disjoining pressure from hard wall

In the absence of the hydration force, i.e. for $V(l) = V_{hw}(l)$, the nonlinear recursion relation leads to an effective potential V_{hw}^{eff} which depends on the roughness $\xi_\perp$ and which behaves as

$$V_{hw}^{eff}(l, \xi_\perp) \approx v_{sc}\,\mathrm{erfc}\left[l/\sqrt{2}\,\xi_\perp\right] \qquad (3.1)$$

for large l where $\mathrm{erfc}[y]$ denotes the complementary error function

$$\mathrm{erfc}[y] = 2\int_y^\infty \frac{dt}{\sqrt{\pi}}\,e^{-t^2}. \qquad (3.2)$$

---

[1] The model as defined by (2.1) has the same form as the so-called solid-on-solid (SOS) models which have been frequently used for two-phase coexistence and crystal growth. The name "solid-on-solid" refers to the fact that the interfacial configurations have no overhangs which is certainly valid for the protrusions considered here. In addition, one has to impose the restriction that $|l_i - l_j|$ is smaller than the length of the lipid molecule which is also fulfilled for the parameter values considered here.

The mean separation ℓ then follows by balancing the external pressure P with the disjoining pressure arising from the hard wall:

$$P = \frac{-\partial V_{\text{hw}}^{\text{eff}}}{\partial l} \approx \frac{\sqrt{2}\, v_{\text{sc}}}{\sqrt{\pi}\, \xi_\perp} e^{-l^2/2\xi_\perp^2} \quad \text{for} \quad l = \ell.$$

(3.3)

The interfacial roughness $\xi_\perp$ is given by

$$\xi_\perp^2 \approx (T/2\pi\Sigma_{\text{pr}}) \ln(\xi_\parallel/a),$$

(3.4)

where a is the diameter of the lipid molecule, and the correlation length $\xi_\parallel$ follows from

$$\frac{\Sigma_{\text{pr}}}{\xi_\parallel^2} = \left.\frac{\partial^2 V_{\text{hw}}^{\text{eff}}}{\partial l^2}\right|_\ell$$

(3.5)

The three equations (3.3)–(3.5) have to be solved selfconsistently. In the limit of small P, one obtains

$$\ell \approx l_{\text{pr}} \left[\ln(P_{\text{hw}}/P) - \tfrac{1}{4}\ln\ln(P_{\text{hw}}/P)\right]$$

(3.6)

and

$$\xi_\perp^2 \approx \tfrac{1}{2} l_{\text{pr}}^2 \ln(P_{\text{hw}\perp}/P),$$

(3.7)

where the protrusion length l_{pr} is given by

$$l_{\text{pr}} \equiv (T/2\pi\Sigma_{\text{pr}})^{1/2}.$$

(3.8)

The pressure amplitudes P_{hw} and $P_{\text{hw}\perp}$ are determined by the requirement that there are no correction terms of order one. The roughness $\xi_\perp$ of the lipid water interface must be small compared to the membrane thickness. This restriction will be discussed in more detail below.

If one inverts the relations (3.6) and (3.7) one arrives at

$$P \approx P_{\text{hw}}\, e^{-\ell/l_{\text{pr}}} (l_{\text{pr}}/\ell)^{1/4}$$

(3.9)

and

$$P \approx P_{\text{hw}\perp}\, e^{-2(\xi_\perp/l_{\text{pr}})^2}.$$

(3.10)

Thus, the protrusion length l_{pr} governs the decay of the disjoining pressure which arises from the renormalization of the hard wall potential by the collective protrusion modes. Note that the continuum model leads to $l_{\text{pr}} = (T/2\pi\Sigma_{\text{pr}})^{1/2}$ whereas the discrete model will give $l_{\text{pr}} \sim l_{\text{sc}} = T/a_0\sigma$.

3.2. Disjoining pressure from hydration interaction

Now, consider potentials of the form $V(l) = V_{\text{hw}}(l) + \Delta V(l)$, where $\Delta V(l)$ contains the hydration interaction as in (1.1). In this case, one may first implement the hard wall potential $V_{\text{hw}}(l)$ into the nonlinear recursion relations and then linearize the resulting RG transformation for $\Delta V(l)$ [16]. In this way, one arrives at the effective potential

$$V^{\text{eff}}(l, \xi_\perp) \approx V_{\text{hw}}^{\text{eff}}(l, \xi_\perp) + \Delta V^{\text{eff}}(l, \xi_\perp),$$

(3.11)

with

$$\Delta V^{\text{eff}}(l, \xi_\perp) \equiv \int_{-y_0}^{y_0} \frac{\mathrm{d}y}{\sqrt{\pi}} e^{-y^2} \Delta V(\sqrt{2}\,\xi_\perp y + l)$$

(3.12)

and

$$y_0 \equiv l/\sqrt{2}\,\xi_\perp.$$

(3.13)

The linear renormalization of $\Delta V(l)$ as described here is somewhat different from the linear recursion relations which have been previously used in the context of wetting [17–19]. In particular, the renormalization group introduced in ref. [18] leads to an effective potential of the same form as in (3.12) but with the upper integration limit y_0 replaced by ∞.

In the present context with $\Delta V(l) = V_{\text{hy}} \exp(-l/l_{\text{hy}})$, one obtains

$$\Delta V^{\text{eff}}(l, \xi_\perp) \approx \tfrac{1}{2} V_{\text{hy}}\, e^{-l/l_{\text{hy}} + \xi_\perp^2/2l_{\text{hy}}^2}$$

$$\times \text{erfc}\left[\frac{-l + \xi_\perp^2/l_{\text{hy}}}{\sqrt{2}\,\xi_\perp}\right]$$

(3.14)

for large l. Now, one may again determine ℓ and $\xi_\perp$ from the relations (3.3)–(3.5) provided $V_{\text{hw}}^{\text{eff}}$ is replaced by $V^{\text{eff}} = V_{\text{hw}}^{\text{eff}} + \Delta V^{\text{eff}}$. The resulting be-
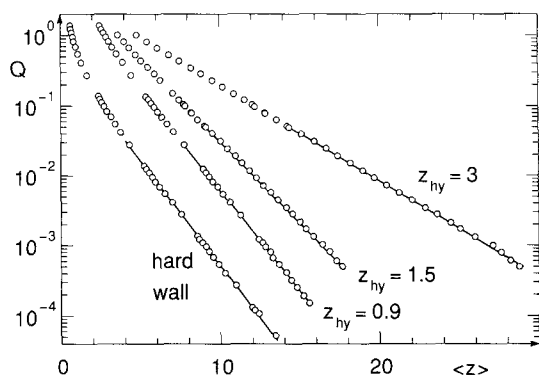
Fig. 2. Monte Carlo data for the reduced pressure $Q = P/P_{sc}$ as a function of the mean separation $\langle z \rangle = \ell/l_{sc}$. Four sets of data are shown (i) for the hard wall potential, and (ii) for the hydration potential (4.2) with $U_{hy} = 13.5$ and different values of the hydration length $z_{hy} = l_{hy}/l_{sc}$. The lines represent fits according to (4.3) and (4.7).

havior depends on the relative size of the two length scales l_{hy} and $l_{pr} = (T/2\pi\Sigma_{pr})^{1/2}$. Indeed, one finds two different scaling regimes: (i) the protrusion regime with $l_{pr} > 2l_{hy}$; and (ii) the hydration regime with $l_{pr} < 2l_{hy}$.

Within the protrusion regime, functional renormalization leads to $\Delta V^{eff}(l, \xi_\perp) \sim \exp(-l^2/2\xi_\perp^2)$ and the asymptotic P dependence of ℓ

and $\xi_\perp^2$ is still given by (3.6) and (3.7) as derived for the hard wall. In the hydration regime, on the other hand, one finds

$$\Delta V^{eff}(l, \xi_\perp) \approx V_{hy}\, e^{-l/l_{hy} + \xi_\perp^2/2l_{hy}^2}. \tag{3.15}$$

The selfconsistent solution now gives

$$P \approx P_2\, e^{-\ell/l_t} \tag{3.16}$$

with the decay length

$$l_t = \left[1 + \left(l_{pr}/2l_{hy}\right)^2\right] l_{hy}. \tag{3.17}$$

The amplitude P_2 is given by

$$P_2 = \left(\Sigma_{pr}/a^2\right)^\rho V_{hy}^{1-\rho} l_{hy}^{2\rho-1} \tag{3.18}$$

with

$$\rho \equiv \left(l_{pr}/l_{hy}\right)^2 / \left[\left(l_{pr}/l_{hy}\right)^2 + 4\right]. \tag{3.19}$$

The roughness $\xi_\perp$, on the other hand, is found to satisfy the relation

$$P \approx P_{2\perp}\, e^{-2\xi_\perp^2/l_{pr}^2} \tag{3.20}$$

with another pressure amplitude $P_{2\perp}$. This relation has the same Gaussian dependence on $\xi_\perp$ as for a hard wall.
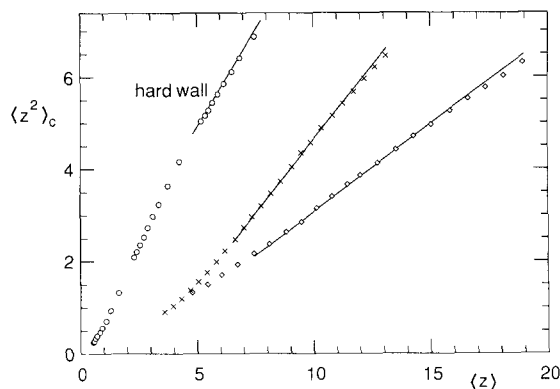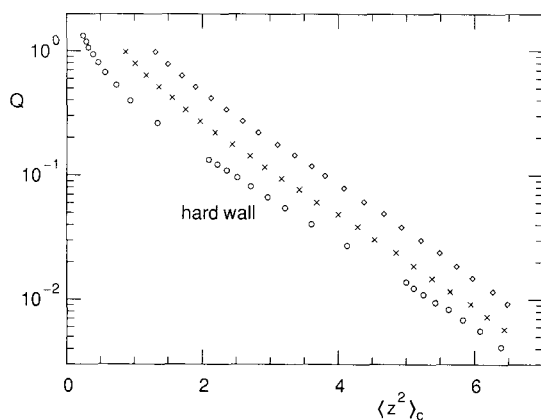

Fig. 3. (a) Monte Carlo data for the reduced pressure $Q = P/P_{sc}$ as a function of the squared roughness $\langle z^2 \rangle_c = (\xi_\perp/l_{sc})^2$. Three sets of data are shown: (i) the hard wall ($\bigcirc$), (ii) the hydration potential (4.2) with $U_{hy} = 13.5$ and $z_{hy} = 1.5$ ($\times$), and (iii) the hydration potential with $U_{hy} = 13.5$ and $z_{hy} = 3$ ($\Diamond$). (b) Monte Carlo data for the squared roughness $\langle z^2 \rangle_c = (\xi_\perp/l_{sc})^2$ as a function of the mean separation $\langle z \rangle = \ell/l_{sc}$. The symbols have the same meaning as in (a). The lines represent fits according to (4.8). The systematic deviation of the data points from these lines for large $\langle z \rangle$ arise from finite size effects.

4. Monte Carlo simulation of discrete interface models

The predictions of functional renormalization as described in the previous subsection can be checked by Monte Carlo studies of the discrete models as given by (2.1) [20]. It will be convenient to use dimensionless variables. Thus, let us introduce the rescaled coordinate $z \equiv l/l_{sc}$ with the scale $l_{sc} = T/a_0\sigma$ as before. One then arrives at the effective Hamiltonian

$$\mathcal{H}\{z\}/T = \sum_{\langle ij \rangle} |z_i - z_j|/n = \sum_i U(z_i) \qquad (4.1)$$

with the rescaled interaction

$$U(z) = Qz + U_{hy} \exp(-z/z_{hy}). \qquad (4.2)$$

This interaction depends on the rescaled pressure $Q \equiv A_0 P/a_0\sigma$ and on the rescaled hydration parameters $U_{hy} \equiv A_0 V_{hy}/T$ and $z_{hy} \equiv l_{hy}/l_{sc}$. Using the values $a_0 \simeq 3$ nm, $A_0 \simeq 0.7$ nm^2 and $\sigma \simeq 0.02$ J/m^2, one obtains the pressure scale $P_{sc} \equiv a_0\sigma/A_0 \simeq 8.6 \times 10^7$ J/m^3, which lies within the range of the experimentally observed values for P_t.

4.1. Disjoining pressure from hard wall

First, let us again consider the case where the interaction $V(l)$ or $U(z)$ does not contain any hydration term, i.e. the case $V_{hy} = U_{hy} = 0$. In this case, the repulsive interaction is determined by the protrusions alone which transform the hard wall into a smoothly decaying potential. The MC data for the mean separation $\langle z \rangle$ and the squared roughness $\langle z^2 \rangle_c \equiv \langle (z - \langle z \rangle)^2 \rangle$ are shown in figs. 2 and 3 for $n = 6$, i.e. for the case of six nearest neighbors per lipid molecule. The data for the mean separation $\langle z \rangle$ can be well fitted to the functional form

$$Q \approx Q_{hw} \, e^{-\langle z \rangle/z_{pr}} (z_{pr}/\langle z \rangle)^{1/4} \qquad (4.3)$$

as follows from (3.9) with $Q = P/P_{sc}$ and $\langle z \rangle = \ell/l_{sc}$. From this fit, the decay length $z_{pr} = l_{pr}/l_{sc}$ and the pressure amplitude $Q_{hw} = P_{hw}/P_{sc}$ are found to be $z_{pr} = 1.54 \pm 0.03$ and $Q_{hw} = 0.51 \pm 0.03$.

The data shown in fig. 2 have been obtained for $(N_\| \times N_\|)$ lattices with $N_\| = 20$ and $N_\| = 40$. These data are not affected by finite size effects over the whole range of Q values as has been checked by additional simulations with $N_\| = 80$. The interfacial roughness, on the other hand, is more susceptible to finite size effects.

Indeed, inspection of fig. 3a shows that the hard wall data for Q as a function of $\langle z^2 \rangle_c$ exhibits a point of inflection which lies in the range $5 \lesssim \langle z^2 \rangle_c \lesssim 6$. For larger values of $\langle z^2 \rangle_c$, the data are curved downwards whereas the asymptotic behavior of $\ln Q$ should be linear as a function of $\langle z^2 \rangle_c$ as follows from (3.10) by rescaling. This downward curvature of the data is an artifact arising from finite size effects.

A simple estimate for the truncation of the accessible $\langle z^2 \rangle_c$ range by finite size effects can be obtained as follows. For periodic boundary conditions as used here, the interface segment becomes strongly correlated as soon as the correlation length $\xi_\|/a$ is comparable to $\frac{1}{2}N_\|$. It follows from (3.4) and $\langle z^2 \rangle_c = (\xi_\perp/l_{sc})^2$ that this limit is reached for

$$\langle z^2 \rangle_c \simeq \langle z^2 \rangle_c^* \equiv z_{pr}^2 \, \ln(\tfrac{1}{2}N_\|). \qquad (4.4)$$

For $N_\| = 20, 40$ and 80 and $z_{pr} = 1.54$, one has $\langle z^2 \rangle_c^* \simeq 5.5, 7.1$, and 8.8, respectively. In practice, finite size effects strongly affect the data for $\langle z^2 \rangle_c$ already for $\xi_\|/a \simeq \frac{1}{4}N_\|$.

If one rescales the result of functional renormalization as given by (3.10), one obtains

$$\ln(Q) \approx \ln Q_{hw \perp} - 2\langle z^2 \rangle_c/z_{pr}^2 \qquad (4.5)$$

for large $\langle z^2 \rangle_c$. Fitting the hard wall data in fig. 3a to this functional form over different ranges of $\langle z^2 \rangle_c$ leads to the estimate $Q_{hw \perp} \equiv P_{hw \perp}/P_{sc} \simeq 0.9$. The quality of this fit has been checked in fig. 3b which shows $\langle z^2 \rangle_c$ as a function of $\langle z \rangle$. Here, a combination of (3.9) and (3.10) leads to

$$\langle z^2 \rangle_c \approx \tfrac{1}{2} z_{pr}^2 \, \ln(Q_{hw \perp}/Q_{hw})$$
$$+ \tfrac{1}{8} z_{pr}^2 \, \ln(\langle z \rangle/z_{pr}) + \tfrac{1}{2} z_{pr}\langle z \rangle. \qquad (4.6)$$

This functional form is used to fit the hard wall data in fig. 3b with the parameter values for z_{pr}, Q_{hw} and $Q_{hw \perp}$ as obtained from the other fits.

4.2. Hydration regime

Several hydration potentials as given by (4.2) with $U_{hy} > 0$ and $z_{hy} > \frac{1}{2}z_{pr}$, $\simeq 0.77$ have also been studied. These potentials belong to the hydration regime for which functional renormalization predicts the non-universal behavior as given by (3.16)–(3.20).

The corresponding MC data for the mean separation $\langle z \rangle = \ell/l_{sc}$ and the squared roughness $\langle z^2 \rangle_c = (\xi_\perp/l_{sc})^2$ are again displayed in figs. 2 and 3, respectively. In this case, the prediction (3.16) of functional renormalization leads to

$$Q \approx Q_2 \, e^{-\langle z \rangle / z_t}, \qquad (4.7)$$

which has been used to fit the $\langle z \rangle$ data in fig. 2. For $U_{hy} = A_0 V_{hy}/T = 13.5$, one then obtains the decay length $z_t = l_t/l_{sc} = 1.53, 1.89, 3.19,$ and 7.60 and the amplitude $Q_2 = P_2/P_{sc} \approx 4.0 \pm 0.7, 5.8 \pm 1.1, 4.4 \pm 0.9,$ and 1.8 ± 0.4 for $z_{hy} = l_{hy}/l_{sc} = 0.9, 1.5, 3,$ and 7.5, respectively. These parameter values are in excellent agreement with the relations (3.17)–(3.19) [7].

The functional dependence of Q on $\langle z^2 \rangle_c$ follows from (3.20). The corresponding fits lead to $Q_{2\perp} \equiv P_{2\perp}/P_{sc} \simeq 1.4$ and 2.5 for $z_{hy} = 1.5$ and 3, respectively. The data for $\langle z^2 \rangle_c$ versus $\langle z \rangle$ as shown in fig. 3b should exhibit the asymptotic behavior

$$\langle z^2 \rangle_c \approx \frac{1}{2} z_{pr}^2 \ln(Q_{2\perp}/Q_2) + \frac{1}{2} z_{pr}^2 \langle z \rangle / z_t. \qquad (4.8)$$

This functional form is represented by the lines in fig. 3b for $z_{hy} = 1.5$ and 3 with the parameter values for z_{pr}, z_t, Q_2, and $Q_{2\perp}$ as determined before.

5. Reduction of bending rigidity by protrusions

A bilayer which exhibits protrusions should be easier to bend than a planar bilayer. Therefore, one would expect that protrusions act to lower the bending rigidity. This reduction will be studied here within a simple continuum model. Thus, consider protrusions from a bilayer which is slightly curved. The bending of the neutral surface of this bilayer is described by $h = h(x)$, the

positions of the two lipid water interfaces bounding the bilayer by $h(x) + l_+(x)$ and $h(x) - l_-(x)$, respectively.

The lipid water interfaces have a certain roughness given by

$$\langle \delta_\pm^2 \rangle \equiv \langle [l_\pm - \langle l_\pm \rangle]^2 \rangle. \qquad (5.1)$$

We will consider the simplest case in which the two monolayers of the bilayer have the same composition, and both interfaces have the same roughness δ with

$$\delta^2 = \langle [l_\pm - \tfrac{1}{2} a_{mem}]^2 \rangle \qquad (5.2)$$

where a_{mem} denotes the thickness of the planar bilayer. The areas $A_\pm$ of the monolayers differ, in general, from the area A of the neutral surface. For small displacements from the planar state, the excess area $\Delta A_\pm \equiv A_\pm - A$ is given by

$$\Delta A_\pm \approx \int d^2 x \left[\tfrac{1}{2} (\nabla l_\pm)^2 \mp l_\pm (\nabla^2 h) \right]. \qquad (5.3)$$

Thus, the elastic energy of the bilayer is taken to be

$$\mathcal{H}_0\{h, l_+, l_-\} = \int d^2 x \, \tfrac{1}{2} \kappa_0 (\nabla^2 h)^2$$
$$+ \Sigma_{pr} (\Delta A_+ + \Delta A_-) \qquad (5.4)$$

where Σ_{pr} again denotes the tension of the lipid water interface arising from protrusions.

It is useful to introduce the new coordinates

$$\delta_1 \equiv \frac{1}{\sqrt{2}} (l_+ + l_- - a_{mem}) \text{ and } \delta_2 \equiv \frac{1}{\sqrt{2}} (l_+ - l_-). \qquad (5.5)$$

The roughness of one of the two lipid water interfaces is now given by $\delta^2 = \frac{1}{2} \langle \delta_1^2 + \delta_2^2 \rangle$.

The displacement field δ_1 describes peristaltic deformations of the bilayer in which this bilayer is compressed and stretched in the transverse direction. We will focus on the limit of low compressibility, for which $l_+ + l_- \simeq a_{mem}$ and thus $\delta_1 \simeq 0$. In this limit, the second displacement field δ_2 describes protrusions of two strongly coupled

lipid water interfaces, and the roughness δ of one of these interfaces satisfies

$$\delta^2 \simeq \tfrac{1}{2}\langle \delta_2^2 \rangle. \qquad (5.6)$$

If the elastic energy (5.4) is expressed in terms of δ_1 and δ_2, one obtains

$$
\begin{aligned}
\mathscr{H}_0\{h, \delta_1, \delta_2\} \\
= \int d^2x \Big\{ \tfrac{1}{2}\kappa_0(\nabla^2 h)^2 - \sqrt{2}\,\Sigma_{\mathrm{pr}}(\nabla^2 h)\delta_2 \\
+ \tfrac{1}{2}\Sigma_{\mathrm{pr}}\big[(\nabla\delta_1)^2 + (\nabla\delta_2)^2\big]\Big\}.
\end{aligned}
\qquad (5.7)
$$

Thus, up to second order in the displacement fields, the height variable h of the neutral surface is only coupled to the displacement field $\delta_2 = (l_+ - l_-)/\sqrt{2}$.

In order to obtain a finite value for the roughness of the lipid water interfaces, one has to add some potentials which confine these interfaces. It is convenient to use the harmonic terms given by

$$\mathscr{H}_1\{\delta_1, \delta_2\} = \int d^2x \big[\tfrac{1}{2}A\delta_1^2 + \tfrac{1}{2}\big(B + 2\Sigma_{\mathrm{pr}}^2/\kappa_0\big)\delta_2^2 \big] \qquad (5.8)$$

The coefficient A must be large in order to attain the limit of small compressibility; its precise value is, however, irrelevant in the present context. The coefficient B, on the other hand, determines the expectation value $\langle \delta_2^2 \rangle \simeq 2\delta^2$. Indeed, after an integration over all configurations of h, one obtains

$$
\begin{aligned}
\langle \delta_2^2 \rangle &= \frac{T}{\Sigma_{\mathrm{pr}}} \int \frac{d^2q}{(2\pi)^2} \frac{1}{q^2 + B/\Sigma_{\mathrm{pr}}} \\
&= \frac{T}{2\pi\Sigma_{\mathrm{pr}}} \tfrac{1}{2}\ln\big(1 + q_{\mathrm{max}}^2 \Sigma_{\mathrm{pr}}/B\big),
\end{aligned}
\qquad (5.9)
$$

where q_{max} is the upper outoff of the q integration. It then follows from $\langle \delta_2^2 \rangle \simeq 2\delta^2$ that

$$q_{\mathrm{max}}^2 \Sigma_{\mathrm{pr}}/B = e^{4\delta^2/l_{\mathrm{pr}}^2} - 1, \qquad (5.10)$$

with $l_{\mathrm{pr}}^2 = T/2\pi\Sigma_{\mathrm{pr}}$ as in (3.8).

Thus, the lipid bilayer is now governed by the effective Hamiltonian $\mathscr{H}_0 + \mathscr{H}_1$ where the parameter B is related to the roughness δ arising from protrusions via (5.10). One may now integrate over all configurations of the displacement field δ_2 which leads to

$$\mathscr{H}_{\mathrm{eff}}\{h\} = \int d^2x \, \tfrac{1}{2}\kappa_{\mathrm{eff}}(\nabla^2 h)^2 \qquad (5.11)$$

with

$$\kappa_{\mathrm{eff}} = \kappa_0/(1 + \Delta) \qquad (5.12)$$

and

$$\Delta \equiv 2\Sigma_{\mathrm{pr}}^2/\kappa_0\big(B + 2\Sigma_{\mathrm{pr}}q^2\big). \qquad (5.13)$$

In the limit of small q, this leads to

$$\Delta \approx \frac{2\Sigma_{\mathrm{pr}}^2}{\kappa_0 B} = 2c_\Sigma (q_{\mathrm{max}} l_{\mathrm{sc}})^{-2}(T/\kappa_0)\big(e^{4\delta^2/l^2} - 1\big), \qquad (5.14)$$

where $\Sigma_{\mathrm{pr}} = c_\Sigma T/l_{\mathrm{sc}}^2$ has been used. Using $c_\Sigma \simeq 0.067$, $q_{\mathrm{max}} = 2\sqrt{\pi}\,/a$, $a = \tfrac{1}{6}\sqrt{3}\,a_0$ (as appropriate for a triangular lattice), one finds

$$\Delta \approx c_\Delta (T/\kappa_0)\big(e^{4\delta^2/l_{\mathrm{pr}}^2} - 1\big), \qquad (5.15)$$

with $c_\Delta \simeq 0.9$ for $a_0 = 3$ nm and $l_{\mathrm{sc}} = 0.1$ nm. This would imply that $\Delta \simeq 0.04$ and 1.21, or $\kappa_{\mathrm{eff}}/\kappa_0 \simeq 0.96$ and 0.45 for $\delta/l_{\mathrm{pr}} = 1/2$ and 1, respectively.

Thus, as soon as the roughness δ of the lipid water interface becomes comparable to the protrusion length l_{pr}, the effective bending rigidity κ_{eff} becomes significantly smaller than the bare rigidity κ_0. In fact, the Gaussian dependence of Δ on δ/l_{pr} as in (5.15) implies that a small increase of δ should lead to a large increase of Δ and thus to a large decrease of κ_{eff}.

6. Summary and outlook

In this paper, we studied the interplay of collective protrusion modes and hydration forces arising from water structure. The roughness of the lipid water interfaces was found to be always small compared to the mean separation of the lipid bilayers, see fig. 3b. Since the relative dis-

placements of the lipid molecules are only of the order of a few Å, the head groups can be treated as rather rigid rods and head group flexibility can be ignored. (The opposite limit of very flexible head groups attached to a planar lipid–solvent interface has been studied by computer simulations in ref. [21]).

The discrete model as given by (2.1) describes the interaction of one protruding and one flat lipid water interface belonging to two different lipid bilayers. For the interaction between two flexible lipid bilayers, there are two changes.

First of all, each bilayer is bounded by two lipid water interfaces. The protrusion of one bilayer will, in general, involve both lipid water interfaces of this bilayer in order to avoid bilayer cavities which would cost a lot of energy. If the bilayer were incompressible, the two lipid water interfaces would have constant separation which would imply that the interfacial free energy for its protrusions is *increased* by a factor of two.

On the other hand, if both bilayers exhibit protrusions, the effective interfacial tension for their *relative* displacement field is *decreased* by a factor of two. Thus, these two effects compensate each other to a certain extent and lead to an overall increase of σ by a factor of $\sqrt{2}$. The finite area compressibility of the bilayer will act to reduce this factor.

In summary, the effective repulsive interaction between lipid bilayers will, in general, depend both on direct hydration forces and on thermally-excited protrusions. Two interaction regimes have to be distinguished depending on the relative size of the protrusion length l_{pr} and of the hydration length l_{hy}. The protrusion length depends on temperature and on the molecular structure of the lipid bilayer, the hydration length on the structure of the solvent.

Within the protrusion-dominated regime with $l_{pr} > 2l_{hy}$, the decay length of the effective repulsive interaction is in fact given by the protrusion length $l_{pr} = z_{pr}l_{sc} = z_{pr}T/a_0\sigma$, see (3.9) and (4.3). Within the hydration-dominated regime with $l_{hy} > \frac{1}{2}l_{pr}$, on the other hand, this decay length is given by $l_t = l_{hy} + l_{pr}^2/4l_{hy} = l_{hy} + z_{pr}^2T^2/4(a_0\sigma)^2l_{hy}$, see (3.17) and (4.7).

At fixed temperature T, the repulsive interac-

tion will be dominated by protrusion and by hydration forces for small and for large values of the parameter $a_0\sigma$, respectively, where $a_0\sigma$ represents an effective edge tension of the lipid molecule. Likewise, protrusion and hydration forces dominate for small and for large values of the hydration length, respectively. Thus, depending on the lipid and on the solvent, a real system may belong to either of both interaction regimes.

For fixed lipid and solvent, on the other hand, one will have a transition at a characteristic temperature $T = T_*$ which is implicitly given by $l_{pr}(T_*) = 2l_{hy}(T_*)$. It follows from the above expressions for these length scales that $T_* = 2a_0l_{hy}\sigma/z_{pr}$ if one ignores the T dependence of the interfacial free energy σ and of the hydration length l_{hy}. For the hydration-dominated regime at low temperatures $T < T_*$, the physical decay length l_t increases quadratically with increasing T, while it increases linearly with T for the protrusion-dominated regime at $T > T_*$.

Protrusions are excitations of the lipid water interfaces which change the interfacial area and are thus governed by an effective interfacial tension. These excitations should be dominant on length scales which are smaller than or comparable with the bilayer thickness. On the other hand, for larger length scales, the typical fluctuations are expected to be bending modes governed by bending rigidity.

A crude estimate for the crossover from protrusion to bending modes can be obtained as follows. For a membrane interacting with a hard wall, protrusions lead to the disjoining pressure $P \approx P_{sc}Q_{hw}\,e^{-\ell/l_{pr}}(l_{sc}/\ell)^{1/4}$ as follows from (4.3) and (3.9). Bending undulations, on the other hand, lead to $P \approx 2c_vT^2/\kappa\ell^3$ with $2c_v = 0.115 \pm 0.005$ (this estimate for c_v follows from fig. 1 of ref [22]). Thus, the exponential dependence of P on ℓ becomes algebraic when ℓ becomes comparable to the crossover scale ℓ_* with

$$e^{-\ell_*/l_{pr}}\left(\ell_*/l_{pr}\right)^{11/4} = 2c_vT^2/Q_{hw}P_{sc}l_{pr}^3\kappa$$
$$= 0.062T^2/P_{sc}l_{sc}^3\kappa. \qquad (6.1)$$

The previous estimates for P_{sc} and l_{sc} lead to $P_{sc}l_{sc}^3 \approx 2.9 \times 10^{-23}$ J. For bending rigidity $\kappa \approx 10^{-19}$ J, one then obtains the crossover scale

$\ell_* \simeq 9.1\ l_{sc}$ at room temperature. For $\ell < l_*$, the disjoining pressure arises primarily from the collective protrusions.

In the presence of a hydration interaction, $V_{hy} \exp[-l/l_{hy}]$, the crossover scale ℓ_* is increased. As an example, consider such an interaction with $l_{hy} = 1.5\ l_{sc} \simeq l_{pr}$ and $V_{hy} = 13.5\ T/A_0$. In this case, the above parameter values lead to the crossover scale $\ell_* \simeq 21.4\ l_{sc}$. For separations $\ell < \ell_*$, the disjoining pressure is governed by the combined effect of collective protrusions and hydration while the bending undulations do not contribute significantly.

It has also been shown in section 5 that protrusions act to reduce the bare bending rigidity. If a single molecule protrudes from the bilayer, it is easier to bend this membrane away from this protrusion. The model introduced in section 5 predicts that this effect is enhanced by collective protrusions. In fact, one finds that the reduction of the bending rigidity depends very strongly on the ratio δ/l_{pr} where δ denotes the roughness of one lipid water interface, see (5.15).

The same considerations apply to surfactant bilayers. Surfactant molecules are typically smaller than lipids and thus characterized by a larger protrusion length. In this case, the roughness δ of the surfactant solvent interface can be enhanced by the addition of cosurfactants. The theory described here then gives a simple explanation for the observed reduction of the bending rigidity.

References

1 R. Lipowsky, Nature 349 (1991) 475; Physica A 194 (1993) 114.

2 J.N. Israelachvili and H. Wennerström, Langmuir 6 (1990) 873.

3 E. Egberts and H.J.C. Berendsen, J. Chem. Phys. 89 (1988) 3718.

4 S. König, W. Pfeiffer, T. Bayerl, D. Richter and E. Sackmann, J. Phys. II (Paris) 2 (1992) 1589.

5 V.A. Parsegian and R.P. Rand, Langmuir 7 (1991) 1299.

6 J.N. Israelachvili and H. Wennerström, J. Phys. Chem. 96 (1992) 520.

7 R. Lipowsky and S. Grotehans, Europhys. Letters 23 (1993) 599.

8 R.P. Rand and V.A. Parsegian, Biochim. Biophys. Acta 988 (1989) 351.

9 J. Marra and J.N. Israelachvili, Biochem. 24 (1985) 4608; J. Marra, J. Colloid Interface Sci. 109 (1986) 11.

10 E. Evans, Coll. Surfaces 43 (1990) 327.

11 R.M. Servuss and W. Helfrich, J. Phys. (Paris) 50 (1989) 809; W. Harbich and W. Helfrich, J. Phys. (Paris) 51 (1990) 1027.

12 R.G. Horn, J.N. Israelachvili, J. Marra, V.A. Parsegian and R.P. Rand, Biophys. J. 54 (1988) 1185.

13 S. Marcelja and N. Radic, Chem. Phys. Letters 42 (1976) 129.

14 G. Cevc, M. Hauser and A.A. Kornyshev, to be published.

15 R. Lipowsky and M.E. Fisher, Phys. Rev. B 36 (1987) 2126.

16 R. Lipowsky, in: Random fluctuations and growth, eds. G. Stanley and N. Ostrowsky (Kluwer, Dordrecht, 1988) p. 227.

17 R. Lipowsky, D.M. Kroll and R.K.P. Zia, Phys. Rev. B 27 (1983) 4499.

18 E. Brezin, B. Halperin and S. Leibler, Phys. Rev. Letters 50 (1983) 1287.

19 D.S. Fisher and D.A. Huse, Phys. Rev. B 32 (1985) 247.

20 G. Gompper, D.M. Kroll and R. Lipowsky, Phys. Rev. B 42 (1990) 961.

21 M.R. Granfeldt and S.J. Miklavic, J. Phys. Chem. 95 (1991) 6351.

22 R. Lipowsky and B. Zielinska, Phys. Rev. Letters 62 (1989) 1572.